Protein Science (1998), 7:2281–2286. Cambridge University Press. Printed in the USA.

Solution structures of stromelysin complexed to thiadiazole inhibitors

BRIAN J. STOCKMAN,[1] DANIEL J. WALDON,[1] JO A. GATES,[1,7] TERRENCE A. SCAHILL,[1] DAVID A. KLOOSTERMAN,[1] STEPHEN A. MIZSAK,[1] E. JON JACOBSEN,[1] KENNETH L. BELONGA,[1] MARK A. MITCHELL,[2] BORYEU MAO,[3] JAMES D. PETKE,[3] LINDA GOODMAN,[4] ELAINE A. POWERS,[4] STEVEN R. LEDBETTER,[4,8] PAUL S. KAYTES,[5] GABRIEL VOGELI,[5] VINCENT P. MARSHALL,[6] GARY L. PETZOLD,[6] AND ROGER A. POORMAN[6]

[1]Structural, Analytical & Medicinal Chemistry, Pharmacia & Upjohn, 301 Henrietta Street, Kalamazoo, Michigan 49001
[2]Medicinal Chemistry, Pharmacia & Upjohn, 301 Henrietta Street, Kalamazoo, Michigan 49001
[3]Computer-Aided Drug Discovery, Pharmacia & Upjohn, 301 Henrietta Street, Kalamazoo, Michigan 49001
[4]Cell and Molecular Biology, Pharmacia & Upjohn, 301 Henrietta Street, Kalamazoo, Michigan 49001
[5]Genomics, Pharmacia & Upjohn, 301 Henrietta Street, Kalamazoo, Michigan 49001
[6]Protein Science, Pharmacia & Upjohn, 301 Henrietta Street, Kalamazoo, Michigan 49001

(RECEIVED February 26, 1998; ACCEPTED July 8, 1998)

Abstract

Unregulated or overexpressed matrix metalloproteinases (MMPs), including stromelysin, collagenase, and gelatinase, have been implicated in several pathological conditions including arthritis and cancer. Small-molecule MMP inhibitors may have therapeutic value in the treatment of these diseases. In this regard, the solution structures of two stromelysin/inhibitor complexes have been investigated using ^{1}H, ^{13}C, and ^{15}N NMR spectroscopy. Both inhibitors are members of a novel class of matrix metalloproteinase inhibitor that contain a thiadiazole group and that interact with stromelysin in a manner distinct from other classes of inhibitors. The inhibitors coordinate the catalytic zinc atom through their exocyclic sulfur atom, with the remainder of the ligand extending into the S_1-S_3 side of the active site. The binding of inhibitor containing a protonated or fluorinated aromatic ring was investigated using ^{1}H and ^{19}F NMR spectroscopy. The fluorinated ring was found to have a reduced ring-flip rate compared to the protonated version. A strong, coplanar interaction between the fluorinated ring of the inhibitor and the aromatic ring of Tyr155 is proposed to account for the reduced ring-flip rate and for the increase in binding affinity observed for the fluorinated inhibitor compared to the protonated inhibitor. Binding interactions observed for the thiadiazole class of ligands have implications for the design of matrix metalloproteinase inhibitors.

Keywords: collagenase; drug design; matrix metalloproteinase; NMR spectroscopy; stromelysin; thiadiazole

Matrix metalloproteinases (MMPs), including stromelysin, collagenase, and gelatinase, are involved in tissue remodeling associated with embryonic development, growth, and wound healing. MMPs are regulated in vivo by selective endogenous tissue inhibitors, TIMPs (Wojtowicz-Praga et al., 1997). Unregulated or overexpressed MMPs have been implicated in several pathological conditions including arthritis and cancer (for recent reviews see MacDougall & Matrisian, 1995; Cawston, 1996). In these cases, where the balance between activated MMP enzymes and endogenous TIMPs is tipped too much in favor of MMP activity, small-molecule inhibitors of stromelysin and other MMPs that mimic the function of TIMPs may have therapeutic value in the treatment of the aforementioned diseases (recently reviewed by Zask et al., 1996).

Knowledge of matrix metalloproteinase structure, especially the ligand binding site, would provide useful information regarding the optimization of lead compounds identified through screening efforts. With this end in mind, a number of NMR and X-ray crystallographic structural studies have been reported on stromelysin (Gooley et al., 1993, 1994, 1996; Van Doren et al., 1993, 1995; Becker et al., 1995; Dhanaraj et al., 1996) and collagenase (Borkakoti et al., 1994; Lovejoy et al., 1994; Reinemer et al., 1994; Spurlino et al., 1994; Stams et al., 1994; Grams et al., 1995;

Reprint requests to: Brian J. Stockman, Pharmacia & Upjohn, 301 Henrietta Street, Kalamazoo, Michigan 49001; e-mail: brian.j.stockman@am.pnu.com.

[7]Present address: Department of Chemistry, University of Illinois, Urbana, Illinois 61801.

[8]Present address: Genzyme Tissue Repair, P.O. Box 9322, Framingham, Massachusetts 01701.

Abbreviations: NOE, nuclear Overhauser effect; NOESY, nuclear Overhauser effect spectroscopy; RMSD, root-mean-square deviation; ROE, rotating-frame Overhauser effect; ROESY, rotating-frame Overhauser effect spectroscopy.

McCoy et al., 1997; Moy et al., 1997) complexed to a variety of inhibitors. The secondary structure and global fold have been found to be quite similar for stromelysin and collagenase and their various complexes with ligands.

These previous studies have involved inhibitors containing either a carboxylate or hydroxamate group that coordinates the active-site zinc atom, such as is the case for PNU-99533 (Spurlino et al., 1994; Stams et al., 1994). With the exception of a Pro-Leu-Gly-hydroxamate inhibitor (Reinemer et al., 1994), the other chemical groups of these inhibitors interact with the S_1'-S_3' binding pockets in the right side of the active site as shown schematically in Figure 1. A highly conserved interaction exists between a hydrophobic group of these right-side binding inhibitors and the deep S_1' pocket.

The structural information presented here describes data from a novel class of MMP binding inhibitors, represented by PNU-107859 (K_i 710 nM) and PNU-142372 (K_i 18 nM), which contain a thiadiazole moiety that coordinates the catalytic zinc atom through its exocyclic sulfur atom. In contrast to other MMP inhibitors (with the exception of the Pro-Leu-Gly-hydroxamate inhibitor), the thiadiazole-containing inhibitors extend into the left side of the active site and interact with the more shallow S_1-S_3 binding pockets as shown schematically in Figure 1. The availability of this structural information provides a unique opportunity to evaluate interactions between MMP inhibitors and the left side of the active site with regard to the design of inhibitors with improved binding strength, or with specificities for different members of the MMP family. Solution NMR studies of stromelysin complexed to PNU-107859 and PNU-142372 are complementary to X-ray crystallographic studies of stromelysin complexed to thiadiazole ligands (Finzel et al., 1998).

RESULTS

Stromelysin/PNU-107859 complex

Sequential main-chain ^1H, ^{13}C, and ^{15}N resonance assignments were made for the stromelysin/PNU-107859 complex by analysis of a variety of three-dimensional data sets. Representative assignment spectra and a summary of resonance assignments are provided as supplementary material.

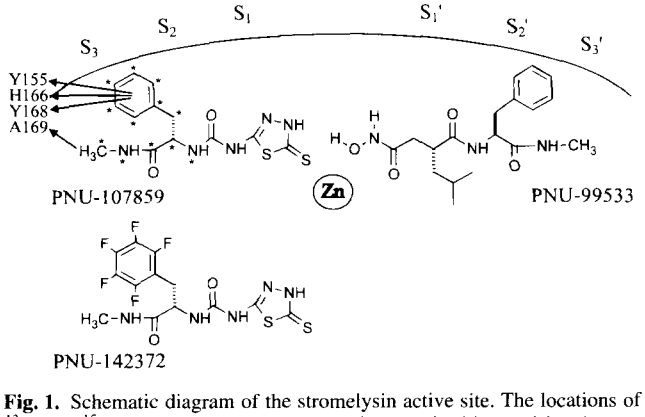

Fig. 1. Schematic diagram of the stromelysin active site. The locations of ^{13}C and ^{15}N labels in PNU-107859 are indicated with asterisks. Arrows indicate interactions between PNU-107859 and protein residues defined by NOEs.

A three-dimensional ^{12}C-filtered, ^{13}C-edited NOESY spectrum recorded on a [^{12}C,^{14}N]PNU-107859/[^{13}C,^{15}N] stromelysin complex was used to assign protein/ligand NOEs. Several two-dimensional ^1H-^1H slices taken at various ^{13}C frequencies are shown in Figure 2. Analysis of this data set was facilitated by prior assignment of the protein $^1H^{\alpha}$, $^1H^{\beta}$, $^{13}C^{\alpha}$, and $^{13}C^{\beta}$ resonances as well as the ligand resonances. Ten NOEs between the ligand and protein aliphatic protons were assigned. Nine involved the aromatic ring of PNU-107859 and one involved the terminal methyl group. NOEs were observed between PNU-107859 and protons of Tyr155, His166, Tyr168, and Ala169. All four of these residues are located in the S_1-S_3 binding sites in the left side of the active site (Fig. 1).

The structure of the stromelysin/PNU-107859 active site as defined by the NMR data is shown in Figure 3. PNU-107859 coordinates the catalytic zinc atom through the exocyclic sulfur atom of the thiadiazole moiety. The planar urea extends away from the thiadiazole ring into the left side of the active site. The extended planarity of the thiadiazole-urea portion would seem to preclude inhibitor binding in the S_1'-S_3' region of the active site since the hydrophobic aromatic group of the ligand would not be positioned to interact in the S_1' pocket. Instead, the aromatic ring of PNU-107859 interacts with the hydrophobic S_3 site formed by the side chains of His166, Tyr168, and Tyr155. Proximity to several protein aromatic groups, especially the Tyr155 aromatic ring, explains the observed ~1 ppm ring-current shifts of the PNU-107859 aromatic resonances upon binding to stromelysin. The interactions of the PNU-107859 aromatic ring with the protein are very similar to those observed for the proline ring of the left-side binding Pro-Leu-Gly hydroxamate inhibitor mentioned earlier (Reinemer et al., 1994). The observation of single resonances for the two $^1H^{\delta}$ and the two $^1H^{\epsilon}$ protons of the PNU-107859 aromatic ring when bound to stromelysin indicates that flipping about the C^{β}-C^{γ} bond

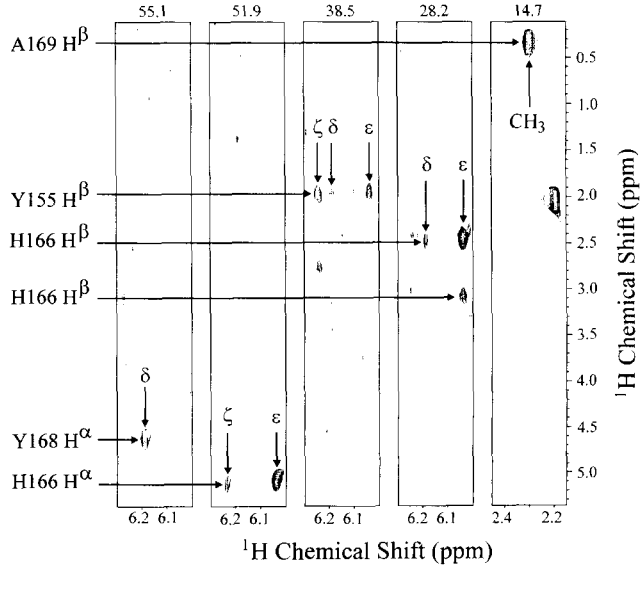

Fig. 2. Two-dimensional ^1H-^1H slices taken from the three-dimensional ^{12}C-filtered, ^{13}C-edited NOESY spectrum of the stromelysin/PNU-107859 complex. Slices correspond to the ^{13}C frequencies indicated at the top. Assigned correlations are labeled according to the protein (horizontal arrows) and ligand (vertical arrows) protons involved.

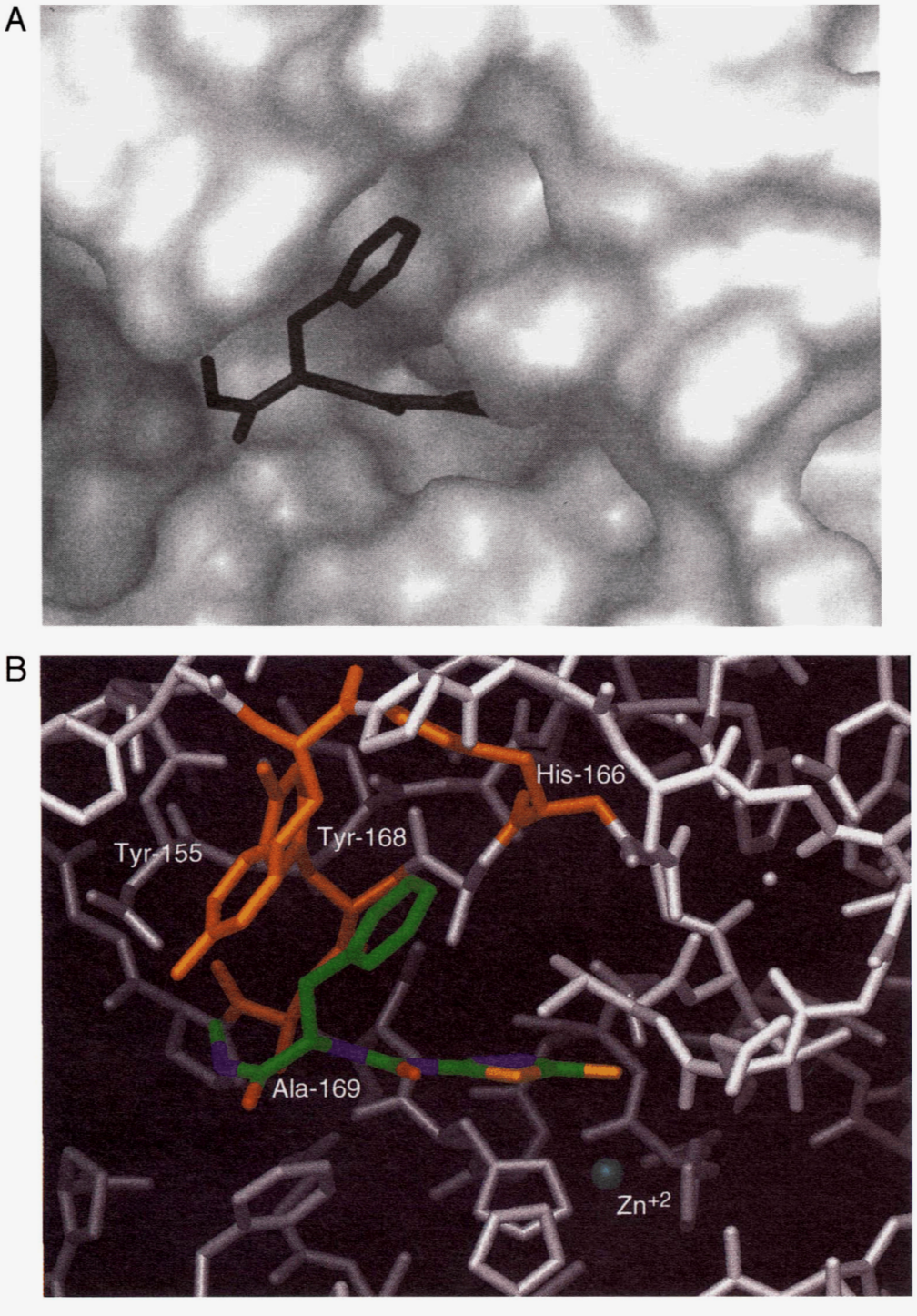

Fig. 3. Solution structure of the stromelysin/PNU-107859 complex. The ligand binding site is shown. **A:** PNU-107859 in tubular format docked into the protein represented by a solid surface. **B:** All-tubular format with protein residues involved in protein/ligand NOEs are shown in orange. PNU-107859 is colored by atom type. The catalytic zinc atom is represented by the turquoise sphere.

is not substantially restricted by interaction of this ring with the S_3 site. The methyl amide carbonyl group of PNU-107859 extends toward and interacts with residues in the S_2 site.

Overall, the final structure is very similar to the initial structure, with an RMSD of 1.86 Å for all backbone atoms. All of the NOE constraints between the protein and PNU-107859 identified in Figure 2 are satisfied. In addition, several protein-ligand NOEs predicted from the coordinates of the final structure are consistent with tentatively assigned resonances. Based on proton–proton distances of <4.0 Å, NOEs are predicted between the methyl, methylene, and aromatic protons of PNU-107859 and the aromatic protons of Tyr155 and Tyr168. However, since these aromatic

protein resonances were not conclusively assigned, NOEs involving them were not used in the calculations. Predicted weak NOEs between the PNU-107859 aromatic protons and the methyl groups of Val163 were not observed experimentally, perhaps because of ligand ring flipping.

The RMSD for the backbone atoms of the stromelysin/PNU-107859 and stromelysin/PNU-142372 (Finzel et al., 1998) structures is 2.07 Å. The two structures agree reasonably well in the active site. However, some differences are observed. In the stromelysin/PNU-107859 structure, the ligand's methyl amide carbonyl group is in the opposite orientation and its aromatic ring is pulled further into the active site. The opposite orientation of the methyl amide carbonyl group results from the fact that either orientation can satisfy the NOE constraint involving the ligand methyl protons. The different binding interactions observed for the ligand aromatic rings may be related to differences in their quadrupole moments as discussed below.

A three-dimensional ^{1}H-^{15}N ROESY-HMQC data set was also recorded on this complex to identify bound water molecules. Fifteen ROE crosspeaks were observed at the water frequency. Five ROE crosspeaks were identified that could not be attributed to either proximity to a rapidly-exchanging side-chain proton or a nonwater proton. These five ROEs involved the backbone amide protons of Arg149, His151, Asp153, Phe154, and Tyr155. An additional seven ROEs involved backbone amide groups that are within 5.0 Å of a rapidly-exchanging side-chain proton. These ROEs involved Thr95, Glu137, Gly159, Thr191, Leu229, Thr230, and Thr255. Two ROEs involving the backbone amide protons of Gly192 and Phe210 could be assigned to $^{1}H^{\alpha}$ protons resonating near the water frequency. The five observed ROEs to bound water were attributed to two bound water molecules that were included in the structure calculations for this complex. The locations of the NMR-identified bound water molecules are shown in Figure 4.

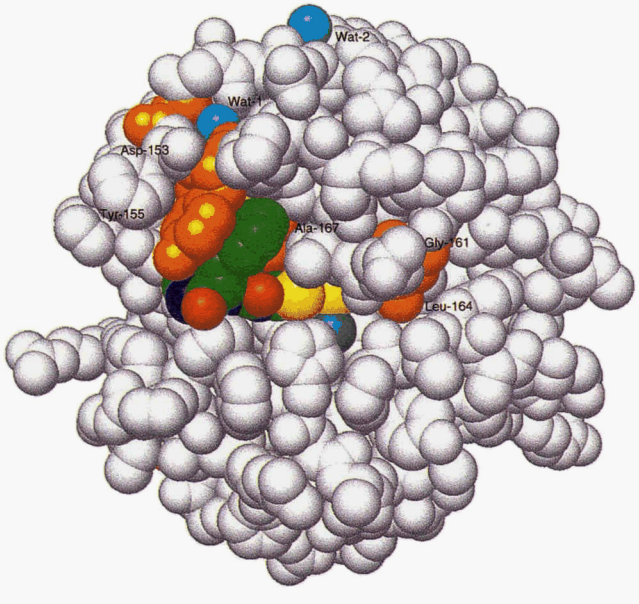

Fig. 4. Space-filling structure of the stromelysin/PNU-107859 complex. PNU-107859 is colored by atom type. The catalytic zinc atom is shown in turquoise beneath PNU-107859. The two bound water molecules are shown in light blue. Residues with the largest differences in ^{1}H and ^{15}N chemical shifts between the stromelysin/PNU-107859 and stromelysin/PNU-142372 complexes are shown in orange and labeled.

Both water molecules are also observed in the X-ray crystallographic structure used as the starting conformation (Becker et al., 1995) and in the X-ray crystallographic structures of two stromelysin/thiadiazole complexes (Finzel et al., 1998). Residues His151, Asp153, Phe154, and Tyr155 form a turn conformation in both the starting and final conformation of the complex. The observed ROEs result from a bound water molecule located in the middle of this turn, labeled Wat1 in Figure 4, corresponding to Wat303 in the starting X-ray crystallographic structure. The ROE to bound water involving Arg149 identifies a second bound water molecule, labeled Wat2 in Figure 4. This water molecule corresponds to Wat354 in the starting X-ray crystallographic structure. The conservation of these two bound water molecules in several stromelysin/ligand complexes confirms that they are structurally important to this region of the protein. Their presence, however, is not dependent on ligand orientation, since they are observed in complexes with the ligand occupying either the S_1-S_3 or S_1'-S_3' binding pockets.

Stromelysin/PNU-142372 complex

Two-dimensional ^{1}H-^{15}N HSQC and three-dimensional ^{1}H-^{15}N NOESY-HSQC spectra were recorded on PNU-142372 complexed to [^{15}N]stromelysin. Sequential main-chain ^{1}H and ^{15}N resonance assignments were made for the stromelysin/PNU-142372 complex by direct comparison of these data sets with those recorded on the stromelysin/PNU-107859 complex. Approximately 90% of the backbone ^{1}H–^{15}N groups had identical chemical shifts in the two complexes. However, a subset of about 20 residues had slight perturbations of their chemical shifts. The pattern of very localized chemical shift changes is similar to what we observed previously in a series of single-site flavodoxin mutants (Stockman et al., 1994). As with flavodoxin, the small change in the chemical structure of the stromelysin/ligand complex induced only localized perturbations in the solution structure. Not including histidine residues, residues that undergo the largest changes in backbone amide group chemical shift are Thr98, Arg134, Asp153, Tyr155, Gly161, Leu164, Ala167, Tyr168, Ala169, and Phe180. Except for Thr98 and Arg134, these residues are concentrated in the active site, especially in the S_1-S_3 pockets of the ligand binding site as shown in Figure 4. Thr98 and Arg134 are located close together on the protein's surface away from the active site. The observed changes in their chemical shifts may reflect small differences in solution conditions between the two complexes. The observed clustering of chemical shift changes in the active site indicates that comparison of protonated and fluorinated versions of a ligand complexed to a receptor may be generally applicable to other systems as well, thus providing a useful tool to identify protein-ligand recognition sites.

The one-dimensional ^{19}F spectrum of the stromelysin/PNU-142372 complex is shown in Figure 5. Distinct resonances are

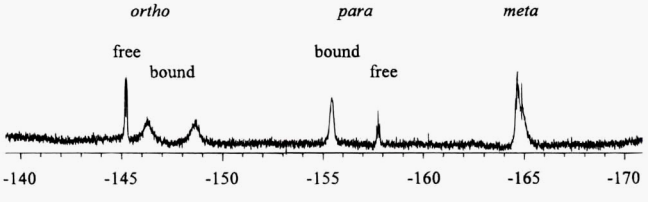

Fig. 5. One-dimensional ^{19}F spectrum of the stromelysin/PNU-142372 complex.

observed for the bound ligand (broad lines) and excess free ligand (sharp lines), as expected for a ligand with an 18 nM binding constant. Unexpectedly, the spectrum contains distinct, resolved resonances for the two ortho fluorine atoms of the bound ligand. A single resonance was observed for the para fluorine atom while the two meta fluorine atom resonances were overlapped in the bound ligand. Usually, the two ortho (and two meta) protons of a symmetric aromatic ring, such as in a phenylalanine or tyrosine residue, will resonate at the same chemical shift. Even though the two individual ortho (and meta) protons experience different environments in the protein structure, and thus, potentially have different chemical shifts, their observed chemical shift is derived from the average of the two environments because of rapid rotation about the C^{β}-C^{γ} bond. The same applies to fluorine atoms on a symmetric aromatic ring. Observation of separate resonances for the two ortho fluorine atoms of stromelysin-bound PNU-142372 is in contrast to the single resonance observed for both ortho protons of stromelysin-bound PNU-107859, indicating that the ring flip rate (rotation about the C^{β}-C^{γ} bond) is reduced for stromelysin-bound PNU-142372 compared to stromelysin-bound PNU-107859. A ring flip rate of approximately 100/s can be estimated from the difference in linewidths for the bound ortho and para fluorine atom resonances (assuming a two-site exchange model). This is at least two orders of magnitude slower than the ring flip rate for PNU-107859, which has been estimated to be >25,000/s.

Discussion

The left-side binding mode of thiadiazole inhibitors was unexpected. In light of the goal to develop potent, broad-spectrum MMP inhibitors, this finding has had profound implications for drug design. To satisfy these criteria, a compound should be active against stromelysin, gelatinase, and collagenase. While PNU-107859 is a good inhibitor of stromelysin (K_i 710 nM), it is a poor inhibitor of gelatinase and is inactive against collagenase. In the case of collagenase, this most likely results from lack of conservation of key protein residues in the left side of the active site. Chief among these are the substitutions of Phe154, Tyr155, Tyr168, and Ala169 in stromelysin with asparagine, serine, phenylalanine, and glutamine, respectively, in collagenase. Collectively, these substitutions result in a much more hydrophilic S_1-S_3 environment in collagenase compared to stromelysin. Efforts to modify PNU-107859 in such a manner as to improve binding to collagenase would most likely reduce affinity for stromelysin. In addition to these differences, the left side of the active site is shallower than the right side, providing fewer possible sites for protein/ligand binding interactions.

The difference in ligand aromatic ring flip rates may be associated with the 40-fold tighter binding of PNU-142372 than PNU-107859 to stromelysin. The reduced ring flip rate in the PNU-142372 complex may arise from steric clashes imposed by the larger size of the fluorinated ring. Favorable hydrogen bonding interactions between the fluorine atoms and nearby bound water molecules may also play a role. More likely, however, the electrostatic interaction between the protein and the aromatic rings of PNU-107859 and PNU-142372 differs. Substitution of the aromatic hydrogen atoms with fluorine atoms has the effect of reversing the quadrupole moment of the aromatic ring. The aromatic ring of PNU-142372 interacts in a parallel-plate fashion (Bovy et al., 1991) with the aromatic ring of Tyr155, as observed in the X-ray crystallographic structure of this complex (Finzel et al., 1998). This type of interaction results because the quadrupole moments of the two aromatic rings are in opposite orientations. This interaction would restrict rotation about the C^{β}-C^{γ} bond in PNU-142372. In the stromelysin/PNU-107859 complex, the interaction between the Tyr155 and ligand aromatic groups is most likely a perpendicular-plate one (Bovy et al., 1991), since the quadrupole moments of the two aromatic rings are in identical orientations. This interaction allows more rapid rotation about the C^{β}-C^{γ} bond.

In this respect, it is interesting to compare the binding affinities and structural observations of the PNU-107859 and PNU-142372 complexes reported here with the binding affinities and structural observations of the PNU-141803 and PNU-142372 complexes (Finzel et al., 1998). In their respective X-ray crystallographic structures, the aromatic rings of PNU-141803 and PNU-142372 are located in the same region of the active site yet interact quite differently with the aromatic ring of Tyr155. The fully-protonated ring of PNU-141803 interacts poorly with Tyr155, while the fully-fluorinated ring of PNU-142372 has an optimal π–π stacking interaction with Tyr155. While there are other differences between PNU-141803 and PNU-142372 and this protein/ligand aromatic/aromatic interaction may not account for the entire difference in binding affinity, the 15-fold affinity difference is comparable to that observed between PNU-107859 and PNU-142372. Incorporation of fluorinated aromatic rings into inhibitors may prove generally useful for improving the potency of other ligands that have aromatic-aromatic interactions with their receptor.

Methods and materials

Structural constraints

Since the highest priority for data analysis was on the active site conformation, structural constraints were concentrated in and around the active site. Our experience with numerous stromelysin/ligand complexes and comparisons to published structures indicates that the nonactive-site regions of stromelysin are nearly identical in each complex. Regions of the starting structure most likely to change conformation during the NMR-based structure refinement calculations are those areas of the protein that interact with ligands. The NMR constraints incorporated for the bulk of the protein thus serve to maintain the elements of secondary structure and the integrity of the metal binding sites during the energy refinement, while the protein-ligand constraints serve to dock the ligand into the active site. Constraints imposed between the protein and the two zinc atoms and three calcium atoms were based on published solution NMR (Gooley et al., 1994) and X-ray crystallographic (Becker et al., 1995) structures of stromelysin.

For the stromelysin/PNU-107859 complex, 541 constraints were used in the structure refinement calculations. These included 356 NOE constraints, 111 distance restraints, and 74 dihedral constraints. Of the 356 NOE-derived constraints, 5 involved constraints between the protein and 2 bound water molecules and 9 involved constraints between the protein and PNU-107859. Of the 111 distance constraints, 90 represented hydrogen bonds inferred from the secondary structure, 13 involved protein-calcium interactions, and 7 involved protein-zinc interactions. For the catalytic zinc atom, one distance constraint involved the exocyclic sulfur atom of PNU-107859. Of the 74 dihedral constraints, 72 represented constraints inferred from the secondary structure and 2 represented constraints to maintain the planarity of the PNU-107859 urea moiety.

Structure calculations

All calculations were run on a Silicon Graphics Indigo2 computer using the program Discover from Molecular Simulations, Inc. (San Diego, California). The starting point for the structure calculations was the coordinates of stromelysin taken from the X-ray crystallographic structure of stromelysin complexed to *N*[1(*R*)-carboxyethyl]-α-(*S*)-(2-phenylethyl)glycine-L-arginine-*N*-phenylamide (Becker et al., 1995). This structure (Protein Data Bank file name: 1SLN) was chosen since it contains two additional calcium atoms compared to the available NMR solution structures. This is critical since one of the additional calcium atoms interacts with residues adjacent to the left side of the binding site and is thus important for maintaining structural integrity during calculations with the thiadiazole inhibitors. After adding protons to the X-ray crystallographic structure, PNU-107859 was manually docked into the binding site in a manner consistent with the pattern of protein/inhibitor NOEs. This starting structure was then subjected to restrained energy minimization and restrained molecular dynamics incorporating the NMR and structural constraints as energy terms. NOEs were classified as strong, medium, or weak. Corresponding upper bound constraints were 3.0, 4.0, and 5.0 Å. The lower bound constraints used in the calculations were the van der Waals contact radii. Force constants used were 40 kcal/mol·Å^2 for distance and NOE constraints and 40 kcal/mol·rad^2 for torsion angle constraints. To limit the movement of atoms from their initial positions, tethering force constants of 500 and 100 kcal/Å were used during energy minimization and molecular dynamics, respectively. All calculations were performed with neutral amino acid side chains using a distance-dependent dielectric constant without a solvation sphere of explicit water molecules. The structure presented here was generated with the following protocol: restrained energy minimization for 100 steps of steepest descents, restrained energy minimization for 500 steps of conjugate gradients, restrained molecular dynamics for 50 ps at 300 K, 5 ps at 285 K, 5 ps at 270 K, 5 ps at 255 K, 5 ps at 240 K, 5 ps at 225 K, 5 ps at 210 K, 5 ps at 195 K, 5 ps at 180 K, 5 ps at 165 K, and 40 ps at 150 K. The final structure contained no distance violations greater than 0.1 Å nor dihedral angle violations greater than 10°. Atomic coordinates for the stromelysin/PNU-107859 complex have been deposited with the Protein Data Bank (3USN).

Electronic supplementary material

Three tables and one text file containing ^{1}H, ^{13}C, and ^{15}N resonance assignments, data acquisition parameters, and sample preparation and NMR data collection methods for both complexes are included. Four figures illustrating the quality of the NMR assignment data are provided.

Acknowledgments

Discussions with Dr. Barry Finzel enhanced the quality of this work and were truly appreciated.

References

Becker JW, Marcy AI, Rokosz LL, Axel MG, Burbaum JJ, Fitzgerald PMD, Cameron PM, Esser CK, Hagmann WK, Hermes JD, Springer JP. 1995. Stromelysin-1: Three-dimensional structure of the inhibited catalytic domain and of the C-truncated proenzyme. *Protien Sci 4*:1966–1976.

Borkakoti N, Winkler FK, Williams DH, D'Arcy A, Broadhurst MJ, Brown PA, Johnson WH, Murray EJ. 1994. Structure of the catalytic domain of human fibroblast collagenase complexed with an inhibitor. *Nat Struct Biol 1*:106–110.

Bovy PR, Getman DP, Matsoukas JM, Moore GJ. 1991. Influence of polyfluorination of the phenylalanine ring of angiotensin II on conformation and biological activity. *Bioch Bioph Acta 1079*:23–28.

Cawston TE. 1996. Metalloproteinase inhibitors and the prevention of connective tissue breakdown. *Pharmacol Ther 70*:163–182.

Dhanaraj V, Ye QZ, Johnson LL, Hupe DJ, Ortwine DF, Dunbar JB Jr, Rubin JR, Pavlovsky A, Humblet C, Blundell TL. 1996. X-ray structure of a hydroxamate inhibitor complex of stromelysin catalytic domain and its comparison with members of the zinc metalloproteinase superfamily. *Structure 4*:375–386.

Finzel BC, Baldwin ET, Bryant GL Jr, Hess GF, Trepod CM, Mott JE, Marshall VP, Petzold GL, Poorman RA, O'Sullivan TJ, Schostarez HJ, Mitchell MA. 1998. Structural characterization of nonpeptidic thiadiazole inhibitors of matrix metalloproteinases reveal the basis for stromelysin selectivity. *Protein Sci 7*:2118–2126.

Gooley PR, Johnson BA, Marcy AI, Cuca GC, Salowe SP, Hagmann WK, Esser CK, Springer JP. 1993. Secondary structure and zinc ligation of human recombinant short-form stromelysin by multidimensional heteronuclear NMR. *Biochemistry 32*:13098–13108.

Gooley PR, O'Connell JF, Marcy AI, Cuca GC, Axel MG, Caldwell CG, Hagmann WK, Becker JW. 1996. Comparison of the structure of human recombinant short form stromelysin by multidimensional heteronuclear NMR and X-ray crystallography. *J Biomol NMR 7*:8–28.

Gooley PR, O'Connell JF, Marcy AI, Cuca GC, Salowe SP, Bush BL, Hermes JD, Esser CK, Hagmann WK, Springer JP, Johnson BA. 1994. The NMR structure of the inhibited catalytic domain of human stromelysin-1. *Nat Struct Biol 1*:111–118.

Grams F, Crimmin M, Hinnes L, Huxley P, Pieper M, Tschesche H, Bode W. 1995. Structure determination and analysis of human neutrophil collagenase complexed with a hydroxamate inhibitor. *Biochemistry 34*:14012–14020.

Lovejoy B, Cleasby A, Hassell AM, Longley K, Luther MA, Weigl D, McGeehan G, McElroy AB, Drewry D, Lambert MH, Jordan SR. 1994. Structure of the catalytic domain of fibroblast collagenase complexed with an inhibitor. *Science 263*:375–377.

MacDougall JR, Matrisian LM. 1995. Contributions of tumor and stromal matrix metalloproteinases to tumor progression, invasion and metastasis. *Cancer Metastasis Rev 14*:351–362.

McCoy MA, Dellwo MJ, Schneider DM, Banks TM, Falvo J, Vavra KJ, Mathiowetz AM, Qoronfleh MW, Ciccarelli R, Cook ER, Pulvino TA, Wahl RC, Wang H. 1997. Assignments and structure determination of the catalytic domain of human fibroblast collagenase using 3D double and triple resonance NMR spectroscopy. *J Biomol NMR 9*:11–24.

Moy FJ, Pisano MR, Chanda PK, Urbano C, Killar LM, Sung M-L, Powers R. 1997. Assignments, secondary structure and dynamics of the inhibitor-free catalytic fragment of human fibroblast collagenase. *J Biomol NMR 10*:9–19.

Reinemer P, Grams F, Huber R, Kleine T, Schnierer S, Piper M, Tschesche H, Bode W. 1994. Structural implications for the role of the N terminus in the 'superactivation' of collagenases. *FEBS Lett 338*:227–233.

Spurlino JC, Smallwood AM, Carlton DD, Banks TM, Vavra KJ, Johnson JS, Cook ER, Falvo J, Wahl RC, Pulvino TA, Wendoloski JJ, Smith DL. 1994. 1.56 Å structure of mature truncated human fibroblast collagenase. *Proteins Struct Funct Genet 19*:98–109.

Stams T, Spurlino JC, Smith DL, Wahl RC, Ho TF, Qoronfleh MW, Banks TM, Rubin B. 1994. Structure of human neutrophil collagenase reveals large S1′ specificity pocket. *Nat Struct Biol 1*:119–123.

Stockman BJ, Richardson TE, Swenson RP. 1994. Structural changes caused by site-directed mutagenesis of tyrosine-98 in *Desulfovibrio vulgaris* flavodoxin delineated by ^{1}H and ^{15}N NMR spectroscopy: Implications for redox potential modulation. *Biochemistry 33*:15298–15308.

Van Doren SR, Kurochkin AV, Hu W, Ye QZ, Johnson LL, Hupe DJ, Zuiderweg ERP. 1995. Solution structure of the catalytic domain of human stromelysin complexed with a hydrophobic inhibitor. *Protein Sci 4*:2487–2498.

Van Doren SR, Kurochkin AV, Ye QZ, Johnson LL, Hupe DJ, Zuiderweg ERP. 1993. Assignments for the main-chain nuclear magnetic resonances and delineation of the secondary structure of the catalytic domain of human stromelysin-1 as obtained from triple-resonance 3D NMR experiments. *Biochemistry 32*:13109–13122.

Wojtowicz-Praga SM, Dickson RB, Hawkins MJ. 1997. Matrix metalloproteinase inhibitors. *Invest New Drugs 15*:61–75.

Zask A, Levin JI, Killar LM, Skotnicki JS. 1996. Inhibition of matrix metalloproteinases: Structure based design. *Curr Pharm Design 2*:624–661.